Non-axisymmetric Stator Design for Boundary Layer Ingesting Fans

Ewan J. Gunn

Turbostream Ltd

3 Charles Babbage Road, Cambridge CB3 0GT, UK

ewan@turbostream-cfd.com

ASME Member

Cesare A. Hall*

Whittle Laboratory, University of Cambridge

1 JJ Thomson Avenue, Cambridge CB3 0DY, UK

cah1003@cam.ac.uk

ASME Member

ABSTRACT

In a Boundary Layer Ingesting (BLI) fan system the inlet flow field is highly non-uniform. In this environment, an axisymmetric stator design suffers from a non-uniform distribution of hub separations, increased wake thicknesses and casing losses. These additional loss sources can be reduced using a non-axisymmetric design that is tuned to the radial and circumferential flow variations at exit from the rotor. In this paper a non-axisymmetric design approach is described for the stator of a low-speed BLI fan. Firstly, sectional design changes are applied at each radial and circumferential location. Next, this approach is combined with the application of non-axisymmetric lean. The designs were tested computationally using full-annulus unsteady CFD of the complete fan stage with a

* Corresponding author

representative inlet distortion. The final design has also been manufactured and tested experimentally. The results show that a 2D sectional approach can be applied non-axisymmetrically to reduce incidence and diffusion factor at each location. This leads to reduced loss, particularly at the casing and midspan, but it does not eliminate the hub separations that are present within highly distorted regions of the annulus. These are relieved by non-axisymmetric lean where the pressure surface is inclined towards the hub. For the final design, the loss in the stator blades operating with BLI was measured to be 10% lower than for the original stator design operating with undistorted inflow. Overall, the results demonstrate that non-axisymmetric design has the potential to eliminate any additional loss in a BLI fan stator caused by the non-uniform ingested flow-field.

INTRODUCTION

Boundary Layer Ingesting (BLI) fan systems interact with the non-uniform inlet flow field, producing a three-dimensional redistribution. This attenuates the axial velocity non-uniformity and leads to swirl and radial angle variations at rotor inlet. As shown in [1], these variations extend around the whole annulus and cause additional loss in the rotor due to the distribution of incidence and loading. The rotor exit flow also has non-uniform swirl and radial angle, which leads to increased losses in the stator row through variations in profile loss and endwall corner separations.

A sketch of the stator exit flow field in a BLI fan is illustrated in Fig. 1. This is based on results presented in [1] and in this paper for a low-speed rig. Similar features have been observed in high-speed fans and compressors operating with inlet total pressure distortion. For example, in [2] full unsteady calculations were performed of a coupled inlet and transonic fan operating with BLI. The fan pressure ratio was 1.35 and the inlet distortion had a similar form to that used in the current study. At exit from the OGV, growing hub separations were visible in the region behind the distorted sector and circumferential variations in the wakes are visible around the annulus. In [3] a low hub-to-tip ratio compressor stage with a pressure ratio 1.5 was tested with a 120° sector inlet total pressure distortion that extended inwards from the casing by 10% span. Computational and experimental results showed high total pressure losses in the stator immediately downstream of the region where the

rotor tip leaves the distorted sector. Increased stator hub and midspan losses were also apparent, even though the inlet distortion was confined to the casing region. In [4] the performance of the NASA rotor 67 stage (fan pressure ratio of 1.63) was studied operating with an inlet square-wave total pressure distortion covering an entire 120° sector. At stator exit, the CFD results revealed large variations in wake thickness around the annulus and large hub separations behind the distorted sector. In this case, the largest casing corner separations were behind the region where the rotor entered the distorted sector. This was also a region of low momentum where the rotor exit swirl angle and stator incidence were high.

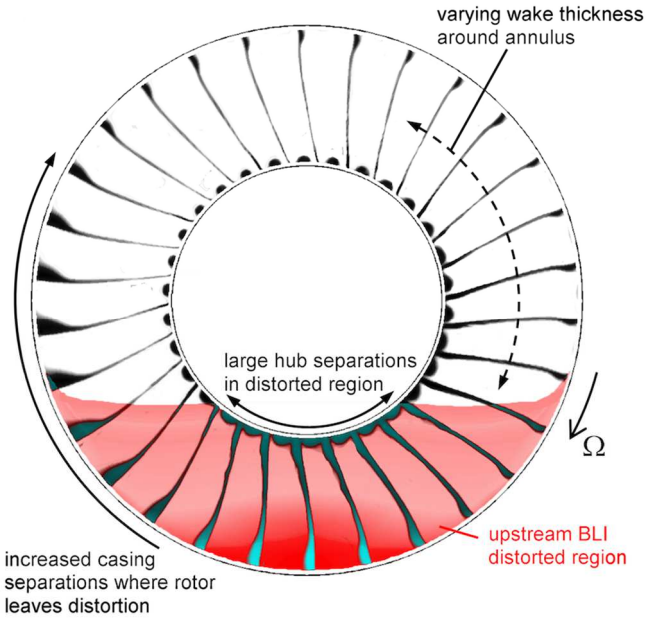

Figure 1: The problem - stator exit wakes for a fan operating within BLI distortion.

It should be possible to design a non-axisymmetric fan stator to compensate for the distorted flow-field and thus minimise the loss sources illustrated in Figure 1. The idea of non-axisymmetric stator design has already been demonstrated in civil turbofans [5]. The upstream static pressure field of a downstream pylon can be eliminated by circumferential variations in stator camber and stagger. However, these variations and the associated distortion are small relative to those associated with BLI. In [6], a non-axisymmetric throughflow method was used to explore the effects of different BLI fan design parameters. It was found that non-axisymmetric stator exit angles could enable favorable rotor

exit static pressure distributions and non-axisymmetric inlet metal angles may be able to mitigate the effect of non-uniformity at stator inlet.

This paper aims to minimise the loss generation in the stator and thus improve the overall stage efficiency of a BLI rig fan. The approach proposed firstly modifies the stator 2D sections, adjusting their incidence and diffusion factor to acceptable values at each radial and circumferential location. This is then combined with the application of non-axisymmetric lean, leading to a 3D redesign which is illustrated in Figure 2. The design changes required are determined using full-annulus unsteady CFD. This form of computation is required to resolve the detailed viscous, three-dimensional flow field and loss variations between each stator passage, which cannot be accurately predicted by a lower fidelity method. The redesigned stator illustrated in Figure 2 has been built and tested experimentally with simulated BLI inlet flow. It is shown to have eliminated the stator casing separations, reduced the stator profile losses and minimised the hub separations. These results prove that the design approach is successful in enabling BLI fan stators to have loss levels comparable to stators operating with clean inflow.

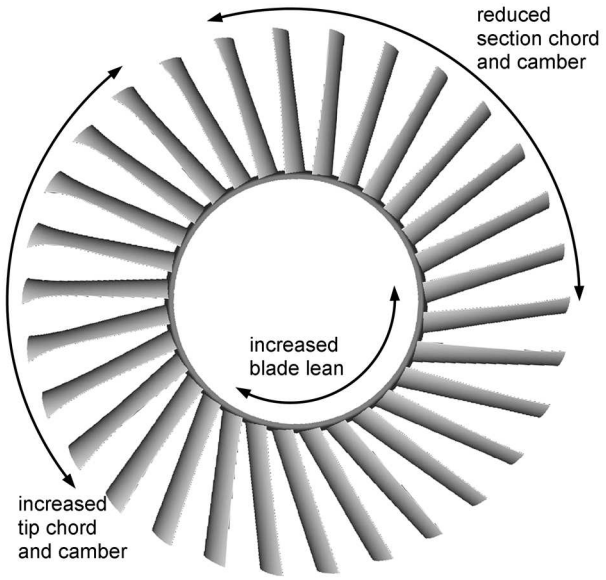

Figure 2: The solution - non axisymmetric stator design with varying camber, chord and lean.

The structure of the paper is as follows: Firstly, the unsteady CFD method and the low speed test rig are described. Secondly, the non-axisymmetric design method is detailed, including the basis of the

design changes and how the geometry, in which all stator blades are different, can be meshed and computed in the CFD. Thirdly, the design approach is applied to the stator of the low-speed BLI fan rig for just 2D non-axisymmetric sectional changes and then for the sectional changes combined with variations in blade lean. Finally, the redesign is tested experimentally and full annulus traverses with a five-hole probe are used to demonstrate improvements in the flow field over the axisymmetric design.

EXPERIMENTAL AND COMPUTATIONAL METHODS

The low-speed BLI fan rig and associated experimental methods are described below, followed by the computational approach used to assess the performance of the fan stage with both axisymmetric and non-axisymmetric stator designs.

Experimental Methods

The experimental rig and test case used in this paper is the low-speed, single-stage fan rig shown in Figure 3 and described in [1,7]. The rig was purpose-built for measuring fan-distortion interaction, with a long intake duct that allows the rotor to interact freely with the distorted upstream flow field. The fan rotor and stator blades were designed for clean inflow with similar velocity triangles to a civil transonic fan. The main design parameters are listed in Table 1.

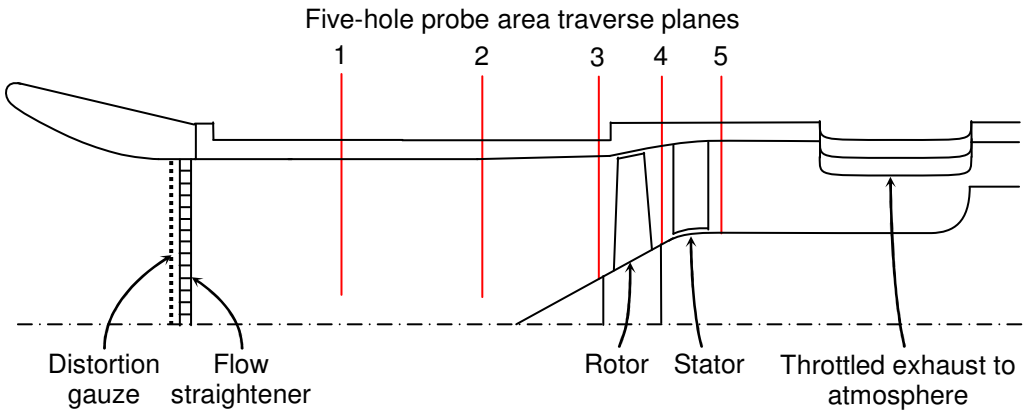

Figure 3: Meridional view of the fan rig showing measurement plane locations.

Flow coefficient	0.50
Stage loading coefficient	0.47
Rotor inlet tip Mach number	0.13
Rotor tip Reynolds number	2×10^5
Rotor inlet hub-to-tip radii ratio	0.3
Rotor inlet tip diameter (m)	0.5
Number of rotor, stator blades	20, 30

Table 1: Key design point parameters for the BLI fan rig.

A stagnation pressure distortion was created in the rig using a gauze at the location shown on Fig. 3. The distortion is representative of the inlet flow within a BLI engine [8], although this method neglects static pressure distortion that may be caused by fan-intake coupling. The gauze was manufactured using a 3D printer as a single sheet with a precisely controlled, non-uniform porosity distribution [1]. The resultant inlet flow field measured with the gauze in place is presented in Figure 4. It is a close match to the target inlet distortion for a BLI engine [8]. The axial velocity varies by a factor of 2 across the inlet duct, and the distortion is equivalent to an ingested boundary layer height of 67% of the fan diameter.

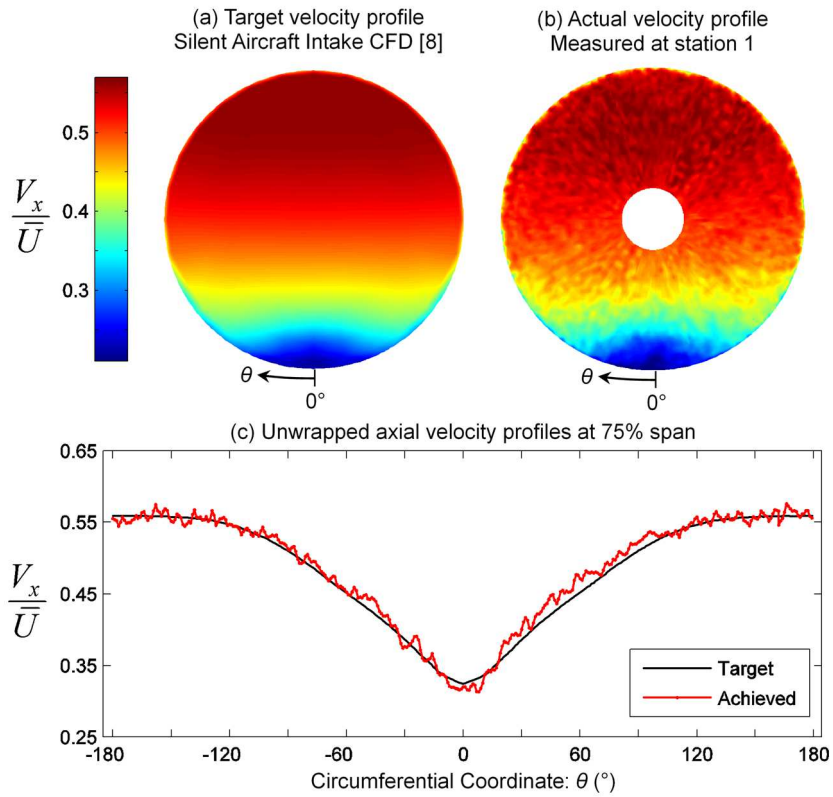

Figure 4: Measured and target inlet velocity profile.

Measurements were carried out with a five-hole pressure probe area traverse system. This paper focuses on the measurements at stations 4 and 5, as indicated in Figure 3. The probe measures the time-averaged stagnation and static pressures and the swirl and radial flow angles. In order to measure accurately within wakes and secondary flow regions, the probe was calibrated to cover a range of swirl and radial angles between -40 and +40 degrees. The area traverse system operates within a 36° sector of the rig. Rotating the inlet distortion relative to this sector allows measurements to be made of the full annulus flow field. Measurements were taken at 34 radial positions and 1° circumferential intervals at station 4. At station 5, the circumferential interval was reduced to 0.5° to enable more detailed resolution of the stator wakes and endwall flows.

To test the final non-axisymmetric stator, the rig had to be fully dismantled after each 36° sector traverse (corresponding to exactly 3 stator pitches). The stator blades and gauze were rotated by 36°, with the rig then being reassembled for the next traverse. The process was repeated ten times to measure the full annulus flow field.

Computational Methods

Full-annulus, unsteady simulations were performed of the complete fan stage operating at the design point with both axisymmetric and non-axisymmetric stator designs. The CFD solver used was Turbostream [9], a 3D, unsteady, Reynolds-averaged Navier Stokes solver running on structured multi-block meshes. The Spalart-Allmaras turbulence model was used [10] and all meshes were created with PADRAM [11].

A 3D image of the CFD domain is presented in Figure 5 with the stagnation pressure distortion from Figure 4 imposed as the inlet boundary condition. Fan-distortion interaction is a long lengthscale problem so it is necessary to use a long computational domain to allow sufficient space for the fan-distortion interaction. In this case the domain extended for 1 diameter upstream and downstream of the fan stage. At exit from the domain a convergent nozzle with a static pressure boundary condition is used to set the fan operating point.

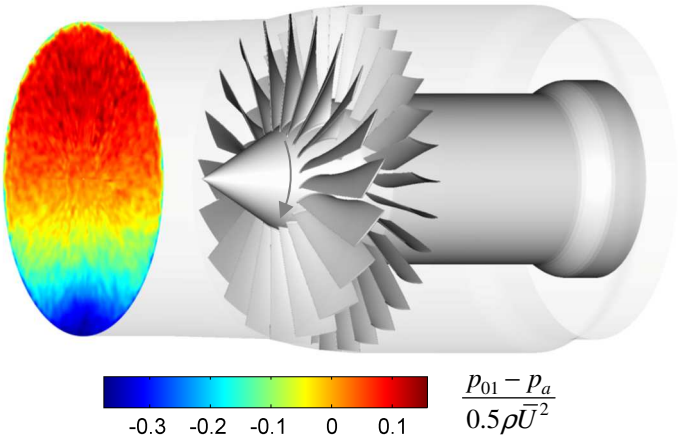

Figure 5: 3D CFD domain for the BLI fan rig operating with the measured inlet stagnation pressure profile.

Approximately 2 million nodes were used per rotor blade passage and the total node count was about 80 million. For the generation and meshing of non-axisymmetric geometry each individual stator blade geometry was converted to a CFD grid. PADRAM [11] was used to combine these into a single grid incorporating all the unique blades. A detailed view of the result is shown in Figure 6 (a). The transition between adjacent blades is smooth, although an increase in clustering occurs between the LE of the largest blades and the upstream sliding plane. However, the axial chord variation was small enough to allow the sliding plane interface to remain at its original location. This meant that no changes had to be made to the inlet, rotor or exhaust grids. A non-axisymmetric grid could therefore be swapped directly into the same computational domain in Figure 5 in place of the original axisymmetric stator grid.

Figure 6 (b) illustrates a sample result of the computed flow-field for the same sector of non-axisymmetric mesh shown in Figure 6 (a). Blade-to blade variations in the stator flow-field are clearly visible including differences in the stator wakes. The rotor wake is transferred smoothly across the sliding plane despite its proximity to the leading edges of the downstream stator blades.

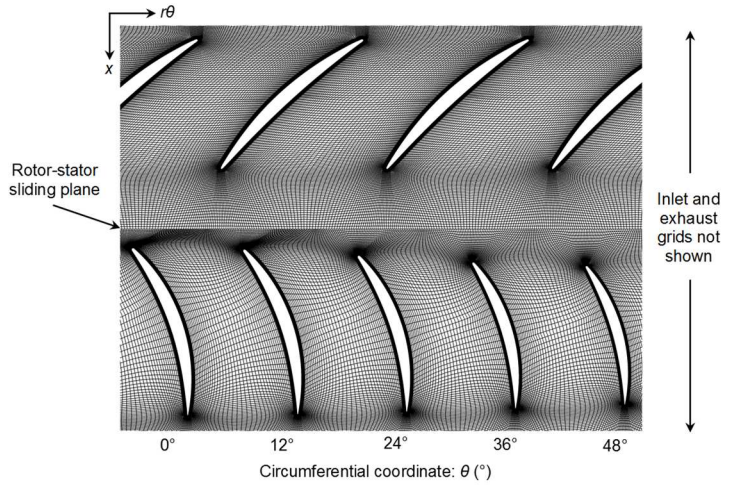

(a) Non-axisymmetric grid

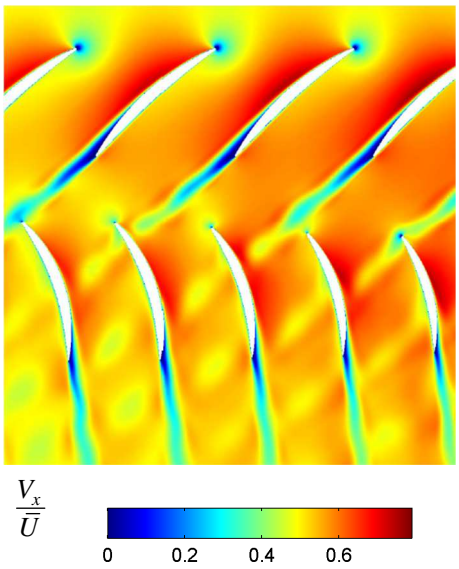

(b) Instantaneous axial velocity

Figure 6: Blade-to-blade view of a mid-span sector of non-axisymmetric grid and flow solution.

FLOW FIELD WITH THE AXISYMMETRIC STATOR

This section details the flow within the BLI rig fan stage when fitted with the baseline, axisymmetric stator. It elaborates on the problems faced by a non-axisymmetric redesign in terms of flow non-uniformity and the distribution of loss sources, and demonstrates the CFD capability to predict the fan flow-field when operating with inlet distortion.

Stator Inlet Conditions

Absolute swirl and radial flow angle distributions at stator exit are plotted in Figure 7 for three spanwise locations for both experiment and CFD. The values are quoted relative to the pitch-wise mass-averaged values in clean flow at the same spanwise positions. These results show how the stator inlet flow field is distorted throughout the annulus. Every stator blade operates at an off-design condition. The circumferential variation of swirl angle, and thus stator incidence, is over 10° at the casing, reducing towards the hub. In contrast, the radial angle variation is almost constant up the span and around 5°. This radial angle variation is a result of the flow redistribution upstream of the rotor, which creates a radial flow that persists throughout the fan stage [1].

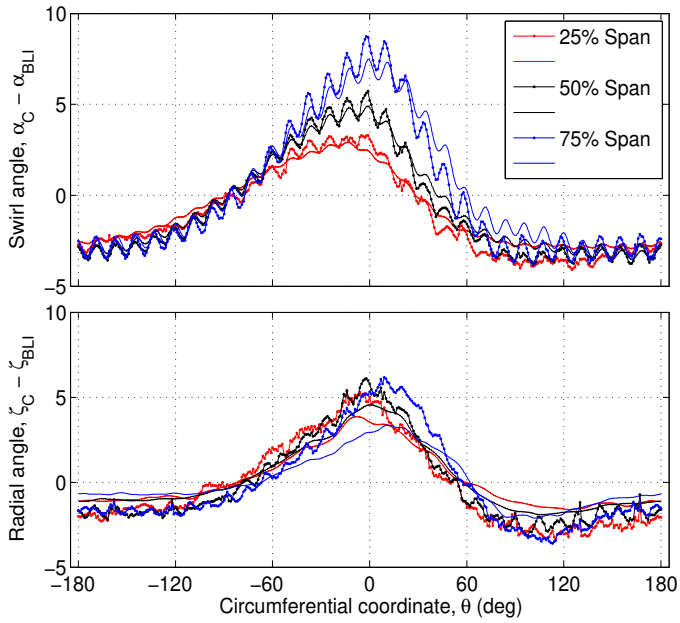

Figure 7: Measured (lines with points) and computed (lines without points) flow angles at stator inlet (station 4).

In both CFD and experiment it was found that the rotor exit relative swirl angle varied by a maximum of 2° circumferentially. This is much smaller than the variation in absolute swirl angle, showing that changes in rotor deviation do not significantly affect the stator inlet flow. The primary source of the variation in stator inlet swirl angle is instead the circumferential variation in mass flux, particularly the low-momentum region near θ = 0°. This region is attenuated by the upstream flow

redistribution, but some low-momentum flow is transferred through the rotor. This is illustrated using velocity triangles in Figure 8. Regions of low axial velocity at rotor exit create a short relative velocity vector, which is overturned upon conversion to the absolute frame. Positive incidence is created and the turning required in the stator increases.

Similar variations in flow angle can be expected for any fan operating within circumferential total pressure distortion. A local deficit in the inlet mass flow can be reduced by the rotor aerodynamics [1], but the rotor exit axial velocity distribution will still be nonuniform, presenting the downstream stator with non-axisymmetric inlet conditions. These can only be addressed using non-axisymmetric design. It is worth noting that in a transonic fan, absolute Mach number variations at rotor exit are also important. In regions of reduced mass flux and higher incidence, the Mach number will be reduced and this could help reduce the stator losses behind the distorted region. Such effects are visible in [1,2,4] and this suggests the amount of non-axisymmetric design variation required in a transonic fan may be lower than for a low speed case.

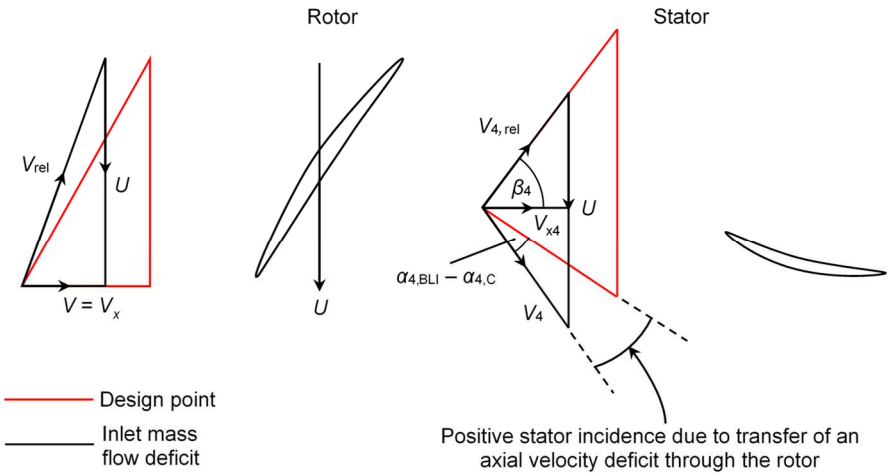

Figure 8: Effect of non-uniform axial velocity on stator incidence in a BLI fan. [1]

Stator Exit Flow Field

For an axisymmetric stator design, the flow angle variations at stator inlet lead to variations in loss. Figure 9 shows contours of stagnation pressure at stator exit for experiment and CFD. Since the flow is incompressible and the stator does zero work, stagnation pressure is a direct measure of loss and the blade wakes are visible as regions of low stagnation pressure. Moving around the

circumference at midspan, the maximum wake thickness occurs within -60° < θ < 30°. This corresponds to upstream locations of high inlet swirl angle, as shown in Figure 7. In contrast, around θ = 180° the wake is thin due to the reduced inlet swirl angle, which leads to lower flow turning through the stator. Note that the asymmetry in the swirl angle distribution shown in Figure 7 is reflected in the wakes, which are generally thinner on the left hand side of the annulus compared with the right.

A band of large casing corner separations can be seen in Figure 9, growing and then shrinking across –30° < θ < 180°. The affected blades lie directly downstream of a region of separated casing flow in the rotor. This is a result of the interaction of the rotor with the inlet distortion [1] and it creates a region of particularly low axial velocity at rotor exit, with correspondingly high swirl angle. The redesign process in the following section will show how these flow separations can be minimised by adjusting the stator blade inlet angle.

The hub endwall flow is different to the casing because the stators are cantilevered with a hub clearance gap of 0.2%. Here the flow is characterised by a small corner separation, influenced by the leakage flow, and by increased profile loss relative to midspan. The size of the hub corner separations increases within the region of high inlet swirl and radial angle in Figure 7 around –60° < θ < 60°.

Figure 9 demonstrates that the CFD reproduces the measured variations in stator wake thickness, casing separations and hub separations. There are differences in absolute terms, particularly in the sizes of the corner separations, which are generally over-predicted by the CFD. However, this is common in CFD predictions of compressor separations and the key finding is that the changes introduced by BLI are captured. Overall, the comparisons shown in Figure 7 and Figure 9 suggest that the CFD can be used as a reliable tool for developing non-axisymmetric stator designs.

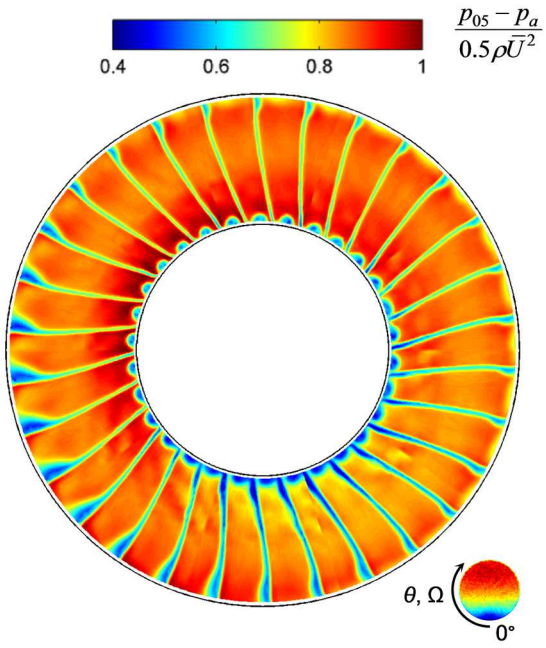

(a) Measured

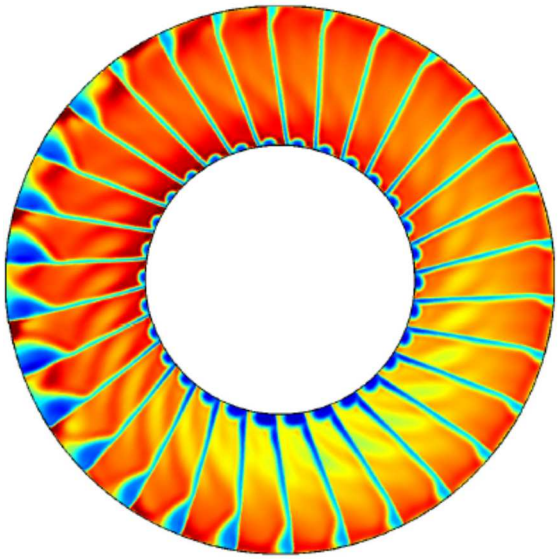

(b) Computed

Figure 9: Measured and computed stagnation pressure distribution at stator exit (station 5).

NON-AXISYMMETRIC REDESIGN

This section describes the approach used to manipulate, define and assess non-axisymmetric stator designs. Non-axisymmetric variations in section parameters are applied first. This is described as a *2D Redesign* because the blade stacking is held constant, although the changes are applied to multiple sections along the span and alter the blade twist. The sectional changes are then combined with non-axisymmetric variations in the stacking lines, which is described as a *3D Redesign*.

Each redesign leads to a set of 30 unique blades which form a non-axisymmetric stator row, in contrast with the baseline design which contained 30 identical blades. The redesigns were tested using full-annulus unsteady CFD at the same BLI operating point described above. The 3D Redesign was also built and tested in the rig, as detailed in the following section.

Blade section parameterisation

The blade section parameterisation was required to provide direct control of the inlet metal angle, axial chord and blade stacking axis, while allowing other aerodynamic parameters to remain fixed. The chosen method was to treat each blade section as a Modified NACA 4-Series aerofoil [12]. These have a second-order polynomial camber line and fourth-order polynomial thickness distribution. This is appropriate for the simple low-speed stator geometry used in the rig. Other machines would require different shapes and in practice, any method that allowed a similar level of control could be used. The section variables detailed in Table 2 are sufficient to fully define a blade section using this method. These are illustrated schematically for an example blade section in Figure 10. The locations of maximum thickness and camber can be varied. The leading and trailing edges are elliptical with variable radius and ellipse ratio and have constraints of constant curvature at the joint with the main part of the aerofoil.

Parameter	Nomenclature	Notes
Inlet angle	χ_{in}	**Design variables**
Axial chord	c_x	
Centroid location	(x_c, θ_c)	**Design variable**
Exit angle	χ_{ex}	Fixed at 0°
Maximum thickness	t/c_x	Held constant
Maximum thickness location	x_{mt}/c_x	
Camber fraction at mid-chord	f_c	
LE radius	r_{LE}	
LE ellipse ratio	R_{LE}/r_{LE}	
TE radius	r_{TE}	
TE ellipse ratio	R_{TE}/r_{TE}	

Table 2: Section design parameters.

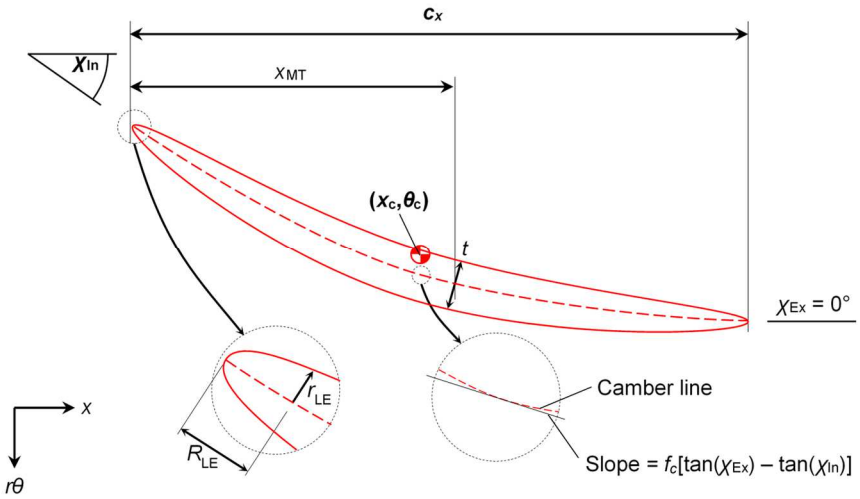

Figure 10: Stator section geometry parameters.

Non-axisymmetric section modification

The results shown in Figure 9 and the study presented in [1] suggest that main drivers of the stator loss variation are the leading edge (LE) incidence and the Lieblein diffusion factor (DF), first defined in [13]. It was hypothesised that the stator loss could therefore be reduced by i) adjusting the inlet metal angle to match the local swirl angle, eliminating the change in LE incidence, and ii) controlling the DF by varying the axial chord to change the pitch-to-chord ratio.

The approach is shown in Figure 11. In areas where the inlet flow angle is high, the inlet metal angle is increased accordingly. These blades will also be subject to high DF values, which can be alleviated by decreasing the pitch-to-chord ratio. This was achieved by increasing the axial chord, because this was the simplest approach and it was not possible to test a design with non-axisymmetric pitch within the existing rig.

In some areas, particularly near, θ = 180°, the stator operates at lower inlet flow angle than in clean flow (see Figure 7). In these regions the inlet angle and axial chord can be decreased to avoid negative LE incidence and excessive wetted area. This has the effect of rebalancing the solidity around the annulus to the areas where it is most needed, which offsets the increased wetted area on the highly loaded blades.

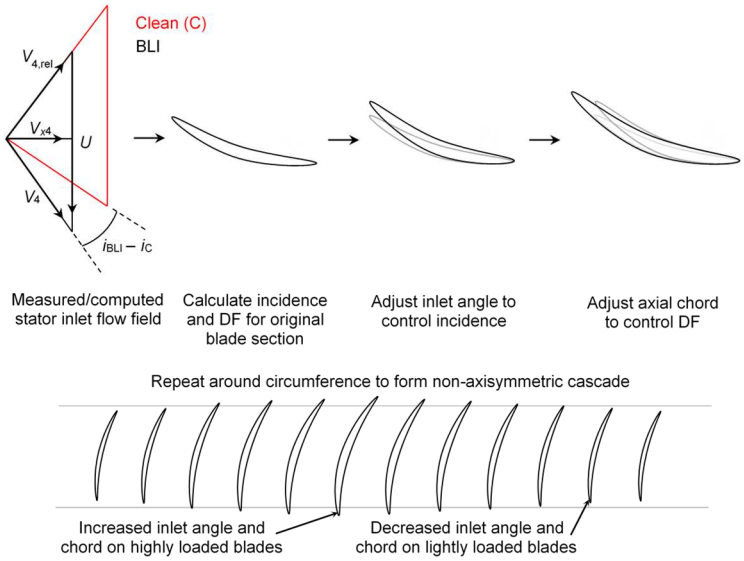

Figure 11: Schematic describing the non-axisymmetric stator section design approach.

The required adjustments in stator inlet metal angle were calculated by simply taking the difference between the rotor exit swirl angle when operating in BLI relative to the original value operating in clean flow:

$$\chi_{New} = \chi_{Base} + \left(i_{BLI} - i_C\right) = \chi_{Base} + \left(\alpha_{BLI} - \alpha_C\right) \tag{1}$$

Near the endwalls the axial velocity is almost zero so the swirl angle is highly sensitive to changes in velocity. This can produce arbitrarily large swirl angle variations at the endwalls. For this reason χ_{New} was limited to a maximum of 55°, a value which was determined by trial and error in the CFD.

The variations in axial chord were determined using the variations in Lieblein's diffusion factor relative to clean flow. The approach was to scale the axial chord according to the measured difference in DF between BLI and clean flow:

$$DF = 1 - \frac{V_5}{V_4} + \frac{1}{2}\frac{\left|V_{\theta 5} - V_{\theta 4}\right|}{V_4}\frac{s}{c} \tag{2}$$

$$c_{x,New} = c_{x,Base} K \left(DF_{BLI} - DF_C\right) \tag{3}$$

The constant K was adjusted to allow a maximum 25% variation in axial chord. This ensured the blade could fit inside the rig between the measurement stations and avoided excessive profile loss.

2D Redesign

Figure 12 shows the resulting variations in inlet angle and chord for a non-axisymmetric design generated following the approach described above and illustrated in Figure 11 (cf. Fig. 7). This design is referred to as the *2D Redesign*. Figure 13 shows the predicted stator flow-field for this design when operating with BLI at the design flow coefficient in Table 1.

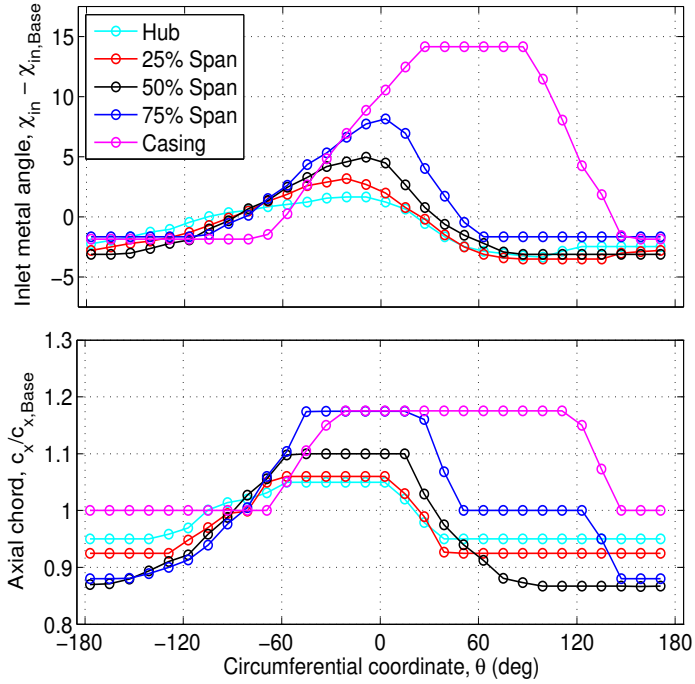

Figure 12: Stator inlet metal angle and axial chord distributions for the 2D Redesign

Comparing Figure 13 with Figure 9(b), this design is successful in reducing the size of casing corner separations on the left side of the annulus while avoiding the introduction of any new corner separations on the right side. Some of the blades on the left side do still show large corner separations. In the CFD the stators were found to be more susceptible to corner separations than in the test and therefore these separations were expected to be an error in the CFD prediction. In fact, the rig test in the following section demonstrates that a similar design minimises the sizes of all the casing separations. It is also evident that the 2D Redesign benefits from reduced wake thickness around midspan near $\theta = 0°$ compared with the axisymmetric baseline. However, there are no favourable changes to the hub separations near $\theta = 0°$. The incidence variation here is relatively low and these separations

are caused by a combination of the 3D flow near the spinner and the low dynamic head of the flow in this region at rotor exit. This means that these separations cannot be strongly influenced using a 2D design approach.

Overall, the application of non-axisymmetric design applied to the blade sections was deemed to be successful in reducing incidence and diffusion. In regions where these factors drive the loss generation, i.e. near the casing and midspan, this leads to corresponding reductions in loss. However, it was not successful in eliminating the hub separations that were particularly 3D in their origin. In the following section, the sectional changes were combined with non-axisymmetric variations in blade stacking to address this.

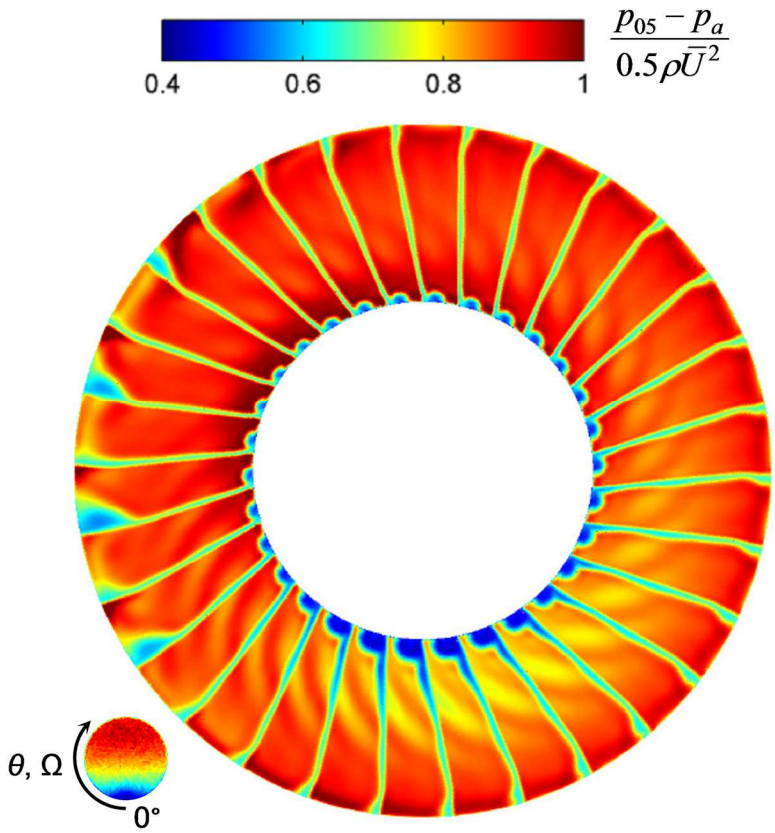

Figure 13: Computed flow field at stator exit for a non-axisymmetric design employing variations in section inlet angle and chord (2D Redesign).

3D Redesign

A study of the effects of different lean options in distorted flow was completed using single-passage steady and full-annulus unsteady CFD. This included varying amounts of end lean, straight lean and compound lean. It is well known [14], that applying pressure surface lean towards the hub reduces hub loading, although this can increase the profile loss further up the span. The objective here was to test if this could deliver an overall benefit in controlling the hub separations evident in Figure 9 and Figure 13.

The most successful approach to non-axisymmetric variable stator stacking was found to be the application of straight lean, so this is the only type presented here. Compared with compound lean, the disadvantage of straight lean is that it cannot improve both endwall flows simultaneously. However, it has the advantage of inducing longer length scale changes in the flow field and it was predicted to be more effective at reducing the size of the hub separations. In CFD studies it was also found to cause less increase in stator profile loss and to have no negative impact on stage efficiency for up to 12° of additional positive lean. Other lean options, when applied in large amounts, were found to cause a reduction in rotor efficiency due to their upstream influence.

The variation in lean applied to the stator in the non-axisymmetric 3D Redesign is illustrated in Figure 14. The distribution was chosen to have a smooth circumferential variation and to have the maximum amount of lean near $\theta = 0°$ where the hub separations are largest. The amount of additional lean varies from 0° to 12° relative to the datum axisymmetric lean value. Lean angles within this range were predicted to have little effect on the clean flow stage efficiency. Any increase in efficiency observed in the BLI design should be attributable to better performance with BLI, and not simply to an improved clean flow stator performance. The 3D Redesign was superimposed on the 2D Redesign and retains the non-axisymmetric sectional parameters shown in Figure 12.

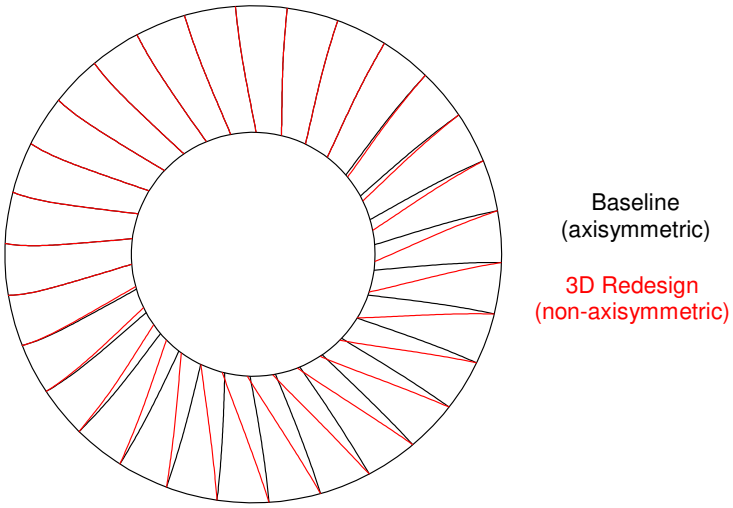

Figure 14: Variation of blade stacking axis for the baseline and the 3D Redesign.

The CFD result for the 3D Redesign operating with BLI at the design flow coefficient is in Figure 15(a). The hub corner separations around $\theta = 0°$ are smaller than the baseline design, Figure 9(b), and significantly smaller than the 2D Redesign, Figure 13. However, this is balanced by an increase in profile loss between 10% and 50% span for $-60° < \theta < 60°$. This is attributed to the fact that, similarly to previous work on lean, localised reductions in loss are offset elsewhere on the blade span. Overall, the integrated value of stagnation pressure loss for the inner 33% of annulus area was predicted to be the same for both the 2D Redesign and the 3D Redesign. There is also a change in the pattern of predicted casing separations, although the CFD is known to be sensitive in this region. The casing separations in Figs. 13 and 15(a) were expected to be smaller in reality, which was proven to be the case when the 3D Redesign was tested (see below).

FLOW FIELD WITH THE NON-AXISYMMETRIC STATOR

In this section, the manufacture and testing is presented for the 3D Redesign presented above. The losses in this design are compared with the original axisymmetric design.

Stator Manufacture and Test

30 individual stator blades were manufactured using rapid prototyping. The tip section of each blade was attached to a one-pitch sector of the casing, which was screwed into an appropriate slot in the rig to fix the blade location. The final assembly is shown in Figure 16.

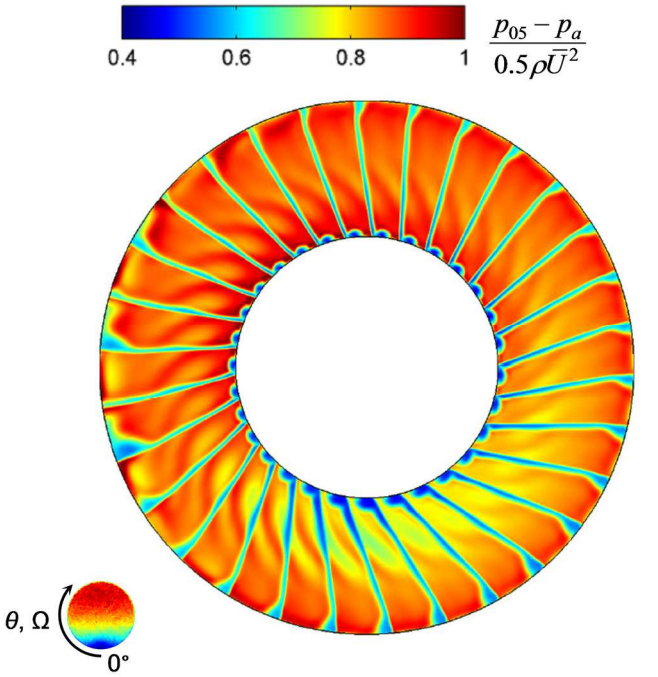

(a) Computed

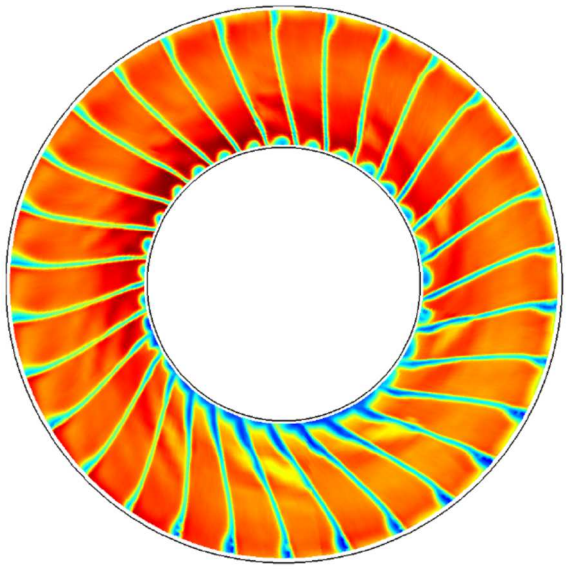

(b) Measured

Figure 15: Computed and Measured stagnation pressure contours downstream of the 3D Re-design.

3D Redesign Measured Flow-Field

The final complete traverse for the exit flow field for the 3D Redesign is presented as Figure 15(b). The results show that the principal effects of non-axisymmetric stator design on the flow-field are captured accurately by the CFD (Figure 15(a)). In addition, the results demonstrate that the non-axisymmetric design methodology is effective.

The most successful aspect of the redesign is the elimination of the casing corner separations on the left side of the annulus. The measurements show that none of the blades in this region have significant separations. This benefit was underpredicted by the CFD, which suggested that a few of these separations would remain. Comparison with Figure 9(a) also confirms a reduction in wake thickness and depth around $\theta = 0°$ away from the endwalls. The changes in the hub flow field are also similar to those predicted by the CFD.

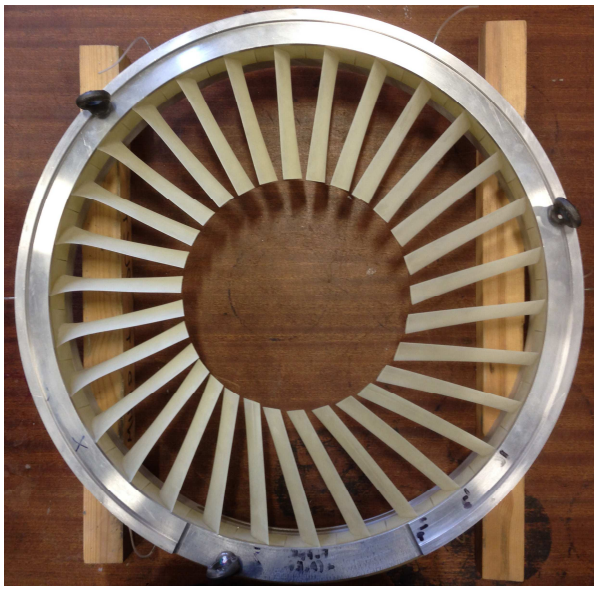

Figure 16: Photograph of the final non-axisymmetric stator assembly (looking aft onto leading edges).

Overall Performance and Stator Comparison

The results in Fig. 17 show that when operating with BLI the non-axisymmetric 3D Redesign has around 25% lower loss than the baseline, axisymmetric design. In fact, the loss is 10% lower than the

baseline design operating in clean flow. This reduction in stator loss is equivalent to an increase in stage efficiency of 0.3%. Some of this improvement could be attributed to the baseline design not being perfectly matched to the clean flow conditions. However, overall this is a clear demonstration that non-axisymmetric design can be used to eliminate any additional stator losses due to BLI.

The measured values differ from the CFD in that they show a larger increase in stator loss due to BLI, but also a larger benefit due to non-axisymmetric design. The differences between the CFD and measurement mainly arise due to the uncertainty in predicted casing separations, where there are the greatest reductions in loss.

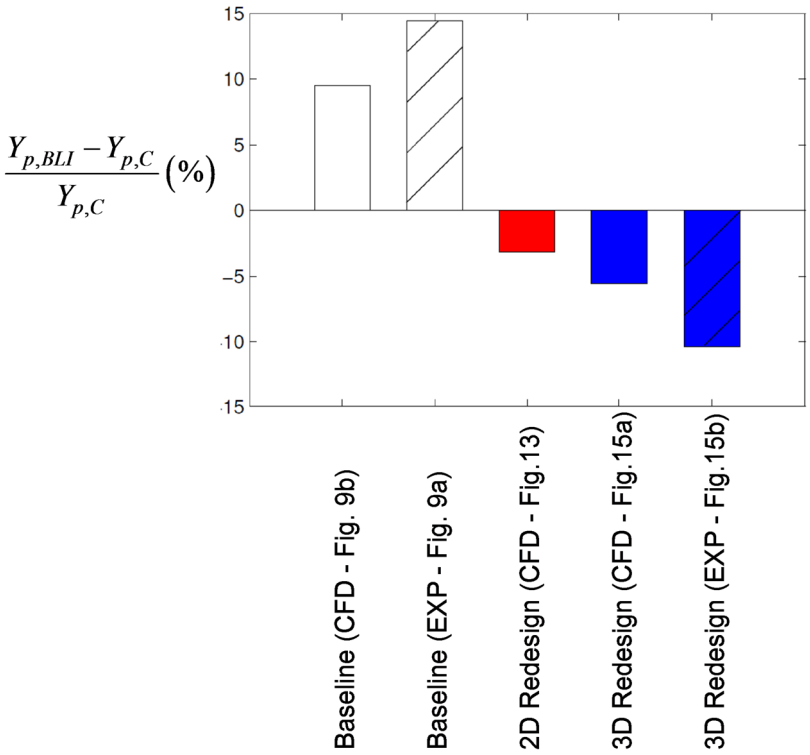

Figure 17: Comparison of overall stator loss coefficients for axisymmetric and non-axisymmetric designs.

CONCLUSIONS

Non-axisymmetric variations in inlet angle and chord are effective at controlling incidence and local diffusion factor in a BLI fan stator. Such variations have been successfully applied and were effective at reducing loss at the casing and midspan in the stator of a low speed rig fan.

The sectional design changes above were found to be less effective where the stator loss is driven by a more 3D flow structure and where the rotor exit flow suffers from a low dynamic head, features which were found to occur near the hub.

Lean with the pressure surface inclined towards the hub, can be applied non-axisymmetrically to suppress regions of hub separations caused by the 3D flow features described above. However, the overall effect on loss may be offset by increased profile loss further up the span.

The final stator design tested has 10% lower loss in BLI than the original stator design has in clean, undistorted inflow. The results demonstrate that non-axisymmetric design can be used to eliminate the additional loss in a BLI fan stator caused by the non-uniform ingested flow-field.

ACKNOWLEDGMENTS

The authors would like to thank Lorenzo Raffaelli and Rolls-Royce plc for supporting and enabling the publication of this work. Turbostream Ltd are acknowledged for making their solver available to the project. Support from EPSRC is also gratefully acknowledged. Colin Bullman provided superb technician support for the operation and modification of the rig. Relevant and useful technical discussions with colleagues Dr Tom Hynes, Prof. Nick Cumpsty, Prof. Rob Miller, Dr Graham Pullan and Dusan Perovic are greatly appreciated.

NOMENCLATURE

Symbols

c	Chord
i	Incidence angle
p	Pressure
r	Radius, Radial coordinate
s	Blade pitch
t	Blade thickness
U	Rotor blade speed

V	Velocity
x	Axial coordinate
Y_p	Stagnation pressure loss coefficient, $\left(\overline{p_{04}} - \overline{p_{05}}\right) \Big/ \frac{1}{2}\rho\bar{U}^2$
α	Absolute whirl flow angle
β	Relative flow angle
ζ	Radial flow angle
χ	Metal angle
Ω	Rotor shaft speed
θ	Circumferential coordinate
ρ	Density
ψ	Pressure rise coefficient

Abbreviations

BLI	Boundary Layer Ingestion
DF	Diffusion Factor

Subscripts

0	Stagnation quantity
1, 2	Values upstream of spinner
3	Value at rotor inlet
4	Value at rotor exit
5	Value at stator exit
mid	Value at mid-span
rel	Relative frame quantity
x	Axial component
θ	Circumferential component

a	Atmospheric value
Base	Baseline design value
BLI	Value in BLI flow
C	Value in clean flow
Ex	Value at stator exit
In	Value at stator inlet
LE	Leading edge value
New	Redesign value
TE	Trailing edge value

REFERENCES

[1] Gunn, E. J. and Hall, C. A. (2014), "Aerodynamics of Boundary Layer Ingesting Fans" in Proceedings of ASME Turbo Expo 2016, Dusseldorf, Germany, GT2014-26142.

[2] Florea, R. V., Voytovych, D., Tillman, G., Stucky, M., Shabbir, A., Sharma, O. and Arend, D. J., 2013, “Aerodynamic Analysis of a Boundary-Layer-Ingesting Distortion-Tolerant Fan,” Proceedings of ASME Turbo Expo 2013, San Antonio, Texas, GT2013-94656.

[3] Wartzek, F., Schiffer, H.-P., Haug, Niehuis, R., J. P., Bitter, M., Kahler, C. J., 2016, “Investigation of Engine Distortion Interaction” in Proceedings of ASME Turbo Expo 2016, Seoul, Korea, GT2016-56208.

[4] Jerez Fidalgo, V., Hall, C. A. and Colin, Y., 2012, “A Study of Fan-Distortion Interaction Within the NASA Rotor 67 Transonic Stage,” Journal of Turbomachinery, 134(5), p. 051011.

[5] Parry, A., 1996. Optimisation of Bypass Fan Outlet Guide Vanes. ASME 1996 International Gas Turbine and Aeroengine Congress and Exhibition, Birmingham.

[6] Hall, D. K., Greitzer, E. M., Tan, C. S., 2017 "Analysis Of Fan Stage Design Attributes For Boundary Layer Ingestion", Journal of Turbomachinery, 139(7), p. 071012.

[7] Perovic, D., Hall, C. A., and Gunn, E. J., 2015. “Stall Inception in a Boundary Layer Ingesting Fan”. In Proceedings of ASME Turbo Expo 2015, Montreal, Canada, GT2015-43025.

[8] Madani, V. and Hynes, T. P., 2009, “Boundary Layer Ingesting Intakes: Design and Optimization,” Proceedings of XIX International Symposium on Air Breathing Engines, ISABE 2009-1346.

[9] Brandvik, T. and Pullan, G., 2011, “An Accelerated 3D Navier-Stokes Solver for Flows in Turbomachines,” Journal of Turbomachinery, 133(2), p. 021025.

[10] Spalart, P. R. and Allmaras, S. R., 1994, “A One-Equation Turbulence Model for Aerodynamic Flows,” La Recherche Aérospatiale, 1 pp. 5-21.

[11] Shahpar, S. and Lapworth, L., 2003, “PADRAM: Parametric Design and Rapid Meshing System for Turbomachinery Optimisation,” Proceedings of ASME Turbo Expo 2003, GT2003-38698.

[12] Jacobs, E.N., Ward, K.E. & Pinkerton, R.M., 1933. The Characteristics of 78 Related Airfoil Sections from Tests in the Variable-Density Wind Tunnel. Report No. 460. National Advisory Committee for Aeronautics.

[13] Lieblein, S., Schwenk, F. C. and Broderick, R. L., 1953, “Diffusion Factor for Estimating Losses and Limiting Blade Loadings in Axial-Flow-Compressor Blade Elements,” National Advisory Committee for Aeronautics (NACA) Research Memorandum, NACA RM E53D01.

[14] Denton, J. D., 2002, “The Effects of Lean and Sweep on Transonic Fan Performance: A Computational Study,” TASK Quarterly, 6(1) pp. 7-24.

Figure Captions List

Fig. 1 The problem - stator exit wakes for a fan operating within BLI distortion

Fig. 2 The solution - non axisymmetric stator design with varying camber, chord and lean

Fig. 3 Meridional view of the fan rig showing measurement plane locations

Fig. 4 Measured and target inlet velocity profile

Fig. 5 3D CFD domain for the BLI fan rig operating with the measured inlet stagnation pressure profile

Fig. 6 Blade-to-blade view of a mid-span sector of non-axisymmetric grid and flow solution.

(a) Non-axisymmetric grid

(b) Instantaneous axial velocity

Fig. 7 Measured (lines with points) and computed (lines without points) flow angles at stator inlet (station 4)

Fig. 8 Effect of non-uniform axial velocity on stator incidence in a BLI fan. [1]

Fig. 9 Measured and computed stagnation pressure distribution at stator exit (station 5).

(a) Measured

(b) Computed

Fig. 10 Stator section geometry parameters

Fig. 11 Schematic describing the non-axisymmetric stator section design approach

Fig. 12 Stator inlet metal angle and axial chord distributions for the 2D Redesign

Fig. 13 Computed flow field at stator exit for a non-axisymmetric design employing variations in sec-tion inlet angle and chord (2D Redesign)

Fig. 14 Variation of blade stacking axis for the baseline and the 3D Redesign

Fig. 15 Computed and Measured stagnation pressure contours downstream of the 3D Redesign

(a) Computed

(b) Measured

Fig. 16 Photograph of the final non-axisymmetric stator assembly (looking aft onto leading edges)

Fig. 17 Comparison of overall stator loss coefficients for axisymmetric and non-axisymmetric designs